SCIENCE CHINA
Earth Sciences

• RESEARCH PAPER •

September 2015 Vol.58 No.9: 1602–1608
doi: 10.1007/s11430-015-5090-x

Statistical characteristics of the equatorial boundary of the nightside auroral particle precipitation

NIU YanYuan[1,2], ZHANG XiaoXin[2*], HE Fei[3] & JIANG Yong[1]

[1] *Nanjing University of Information Science & Technology, Nanjing 210044, China;*
[2] *Key Laboratory of Space Weather, National Center for Space Weather, China Meteorological Administration, Beijing 100081, China;*
[3] *Changchun Institute of Optics, Fine Mechanics and Physics, Chinese Academy of Sciences, Changchun 130033, China*

Received December 21, 2014; accepted February 18, 2015; published online May 7, 2015

Based on the auroral electron/ion precipitation boundary database observed by the DMSP satellites during 1984–2009, the characteristics of the nightside equatorial boundaries of the electron precipitation (B1E) and the ion precipitation (B1I) in the Northern/Southern Hemispheres (NH/SH) are statistically investigated. The results show: That most of the boundaries are located between magnetic latitude (MLAT) of 60°–70° with the mean MLAT for B1E/B1I to be 64.30°N/63.22°N and 64.48°S/63.26°S in the NH and SH, respectively, indicating that B1E and B1I in both hemispheres are located in conjugated magnetic field lines with B1E ~1.2° poleward of B1I; that the MLAT of B1E and B1I in both hemispheres shift to lower MLAT (from ~70° to ~55°) as geomagnetic activity increases; that MLAT of both B1E and B1I and their differences slowly decrease from dusk to midnight with some difference in both hemispheres during different levels of geomagnetic activities; that B1E and B1I in both hemisphere decrease linearly with *Kp* and exponentially with *Dst*, *AE*, and *SYM-H*, respectively, demonstrating that auroral particle precipitation is closely related with geomagnetic activity; that in different magnetic local time (MLT) sectors, the changing rates of the boundaries with *Kp* are different, and the rates of B1E are generally larger than that of B1I, implying that the difference between B1E and B1I reduce with increasing geomagnetic activity. Compared with previous studies, the statistical results based on the long-term large database in this paper can well reflect the properties of the equatorial boundaries of auroral precipitation and may be used for physical modeling or space weather forecasting in future.

auroral particle precipitation, equatorial boudanry, statistical characteristics, geomagnetic activity

Citation: Niu Y Y, Zhang X X, He F, Jiang Y. 2015. Statistical characteristics of the equatorial boundary of the nightside auroral particle precipitation. Science China: Earth Sciences, 58: 1602−1608, doi: 10.1007/s11430-015-5090-x

The Earth's magnetosphere, which has very complex magnetic field structures and plasmas with wide range of density, is the plasma region that surrouds the Earth and is controlled by geomagnetic field. During solar eruptions, espacially during solar maximum when solar flare, solar coronal mass ejection, or solar wind high-speed flow happen more frequently, the mass, energy, and interplanetary magnetic field carried by the solar wind can be transformed into the magnetosphere where the current systems are disturbed to form the geomagnetic storm that effects geospace. During geomagnetic disturbances, energetic particles in the magnetosphere can precipitate into the high-latitude ionosphere along geomagnetic field lines and form aurora with different patterns. The poleward boundary of the aurora is at magnetic latitude (MLAT) of ~80°, corresponding to the outer boundary of the plasma sheet, also the boundary of polar cap, and the equatorward boundary of the aurora is at MLAT of ~65°, corresponding to the outer boundary of the plasmasphere (Xu, 2009). The configuration of the boundaries is a good indicator of the magnetosphere-ionosphere coupling and has been paid

*Corresponding author (email: xxzhang@cma.gov.cn)

many attentions in space physics research community. These boundaries can help us establish a clear picture of magnetospheric particle penetrating to auroral ionosphere.

The auroral boundaries can be identified from the observations of auroral particle precipitations from low-altitude satellites. These boundaries, including poleward and equatorial boundaries, exhibit different patterns in the auroral region which reflect different origin of the particles from the magnetosphere. This most important is that, the nightside boundaries are directly associated with the difference between the location of the inner edge of the electron and ion plasma sheet populations, reflecting the coupling processes in the nightside magnetosphere and ionosphere. Newell et al. (1996, 2004) and Feldstein et al. (1996) have proposed an automatic identification method to extract the nightside boundaries. The equatorial boundary of electron precipitation is commonly termed as "zero-energy" (refer to very low energy) convection boundary (B1E), usually corresponds to plasmapause (Horwitz et al., 1986; Anderson et al., 2008), since zero-energy particles have no curvature and gradient drift. Similarly, the ion precipitation also has "zero-energy" boundary (B1I) (Gussenhoven et al., 1983; Nakai et al., 1986). Such low energy boundaries usually move toward equator with increasing geomagnetic activity and are used for space weather forecast.

The characteristics of the equatorial boundary of the particle precipitation to auroral region have been studied by many works, and most of these studies focus on the correlations of the equatorial boundaries to geomagnetic activities (Gussenhoven et al., 1981, 1983, 1987; Feldstein et al., 1985; Horwitz et al., 1986; Nakai et al., 1986; Anderson et al., 2008). For example, Gussenhoven et al. (1987) studied the differences, the magnetic local time (MLT) variations and the geomagnetic activity variations of the equatorial boundaries of the ion and electron precipitations based on the observations by the precipitating energetic particle spectrometer (SSJ/4) on DMSP F6. Limited by the orbit of F6, only the boundaries in 04:00–07:00 MLT and 17:00–21:00 MLT are investigated. They have found that the average MLAT of the electron boundary is 2.6° larger than that of the ion boundary with many cases larger than 5° in the dusk/evening sectors, and the difference is 1.4°–3° in the dawn/morning sectors. Both the electron and ion boundaries move to low latitudes with increasing geomagnetic activity measured by *Kp* and the differences between electron and ion increase when MLT increases from midnight to noon. These works are only based on limited temporal and/or spatial coverage of database and the picture of the equatorial boundary of the particle precipitation to auroral region has not been fully understood.

In this study we use the Defense Meteorological Satellite Program (DMSP) precipitating ion and electron data to study the characteristics of the nightside equatorial boundaries of the electron precipitation (B1E) and the ion precipitation (B1I) in the Northern/Southern Hemispheres (NH/SH). The large database used in this paper covers years between 1984 and 2009 and are for the first time used to extract B1E and B1I and to study their correlations with geomagnetic activity. It is expected that the statistical results based on the long-term large database can well reflect the properties of the equatorial boundaries of auroral precipitation associated with dependence on geomagnetic activity.

1 Data and method

According to the observations by the precipitating energetic particle spectrometer (SSJ/4 and SSJ/5) (Hardy et al., 1984) on the Defense Meteorological Satellite Program (DMSP), Newell et al. (1991) extracted the various boundaries in auroral oval based on pattern recognition technique (neural network), and the universal time (UT), location, average flux and peak flux for these boundaries are picked up to establish an online database (http://sd-www.jhuapl.edu/Aurora/dataset_list.html) covering years of 1984–2009.

As an example, Figure 1 shows a DMSP F13 cross in the nightside in the Northern Hemisphere on August 28, 2004. A sharp boundary equatorward of the auroral precipitation where the total energy flux decreases by more than one order can clearly be seen in Figure 1 for both electron and ion precipitations, as marked by the vertical black lines (B1E) and the vertical red lines (B1I). Then, the UT, MLAT, and MLT of the nightside boundaries are extracted and matched with *Kp*, *Dst*, *AE*, and *SYM-H* indices to form a new database which includes B1E and B1I in both hemispheres. In the new database, B1E samples are 273415 (NH) and 346298 (SH), and B1I samples are 244141 (NH) and 296955 (NH), respectively. The geomagnetic indices are provided by Kyoto World Data Center. Based on this new database, the distribution characteristics, MLT variations, and geomagnetic variations of the B1E and B1I in both hemispheres will be systematically investigated.

2 Database information

Figure 2 shows the basic information of the database versus MLAT, MLT, year, and DOY. It is revealed in Figure 2(a) that most of the boundaries are located between 60°–70°, with the mean MLAT for B1E/B1I to be 64.30°N/63.22°N in NH and 64.48°S/63.26°S in SH, respectively. This indicates that both the B1E and B1I in NH/SH are located in conjugated magnetic field lines and the MLAT of B1E is ~1.2° larger than that of B1I, which is in consistent with the results by Gussenhoven et al. (1987). Figure 2(b) shows that little boundaries are detected around 01:00 MLT due the fact that all of the DMSP orbits are located in the dawn/dusk or morning/evening sectors. The distribution patterns in Figure 2(c) and (d) are determined by the number of satellites that are simultaneously in orbits.

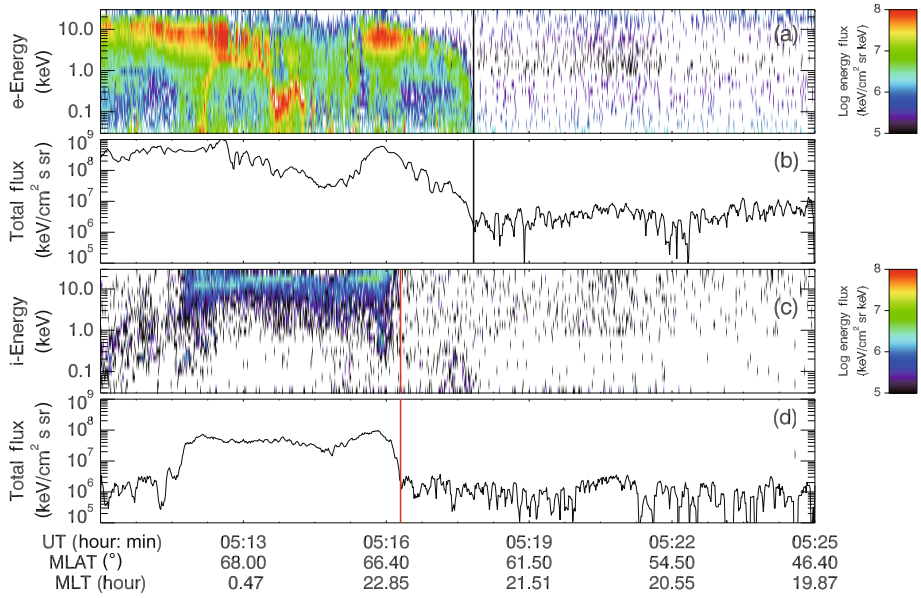

Figure 1 An example of DMSP F13 SSJ/4 observation on August 28, 2004. (a) Precipitating electron energy flux; (b) total electron flux; (c) precipitating ion energy flux; (d) total ion flux. The vertical black lines in (a) and (b) represent the equatorial boundary of precipitating electrons (B1E), and the vertical red lines in (c) and (d) represent the equatorial boundary of precipitating ions (B1I).

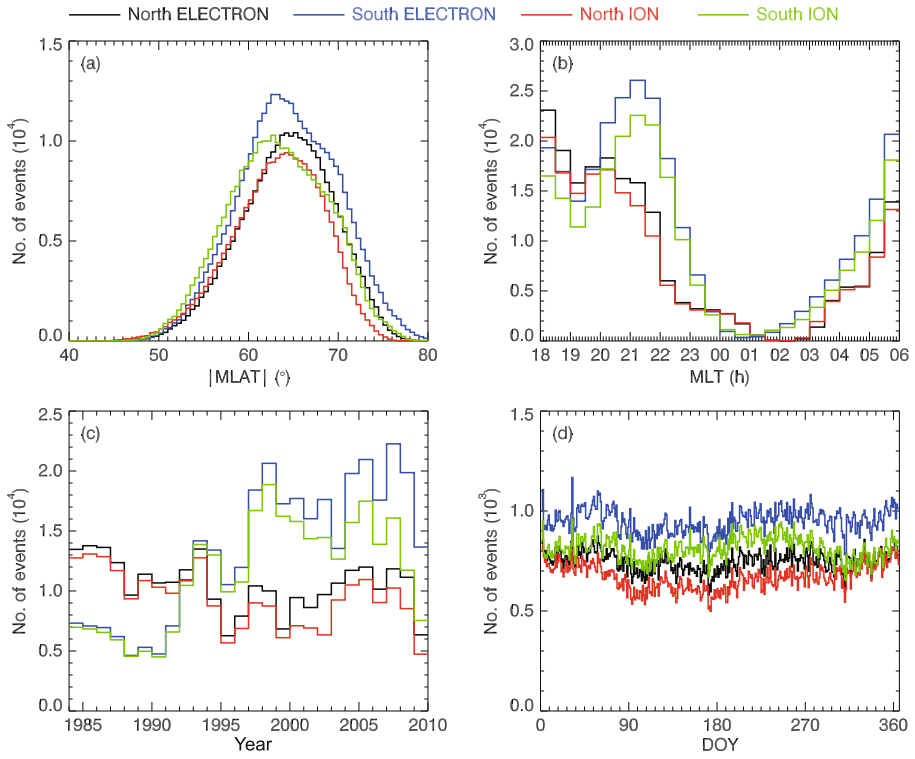

Figure 2 Number of the events of B1E (black/blue) and B1I (red/green) in NH/SH hemisphere versus. (a) |MLAT| (binned in 0.5° intervals); (b) MLT (binned in 0.5 h intervals); (c) year (binned in 1 year intervals); (d) day of year (DOY, binned in 1 day intervals). The colors representing different boundaries are shown at top.

The distribution of events with *Kp*, *Dst*, *AE*, and *SYM-H* indices are displayed in Figure 3. In both hemispheres, 90% of the events happen when *Kp* is less than 4.0, *Dst* is greater than −100 nT, *SYM-H* is greater than −100 nT, and *AE* is less than 600 nT. The number of events decreases dramatically with geomagnetic activity because that the quiet periods are significantly much more than the disturbed periods.

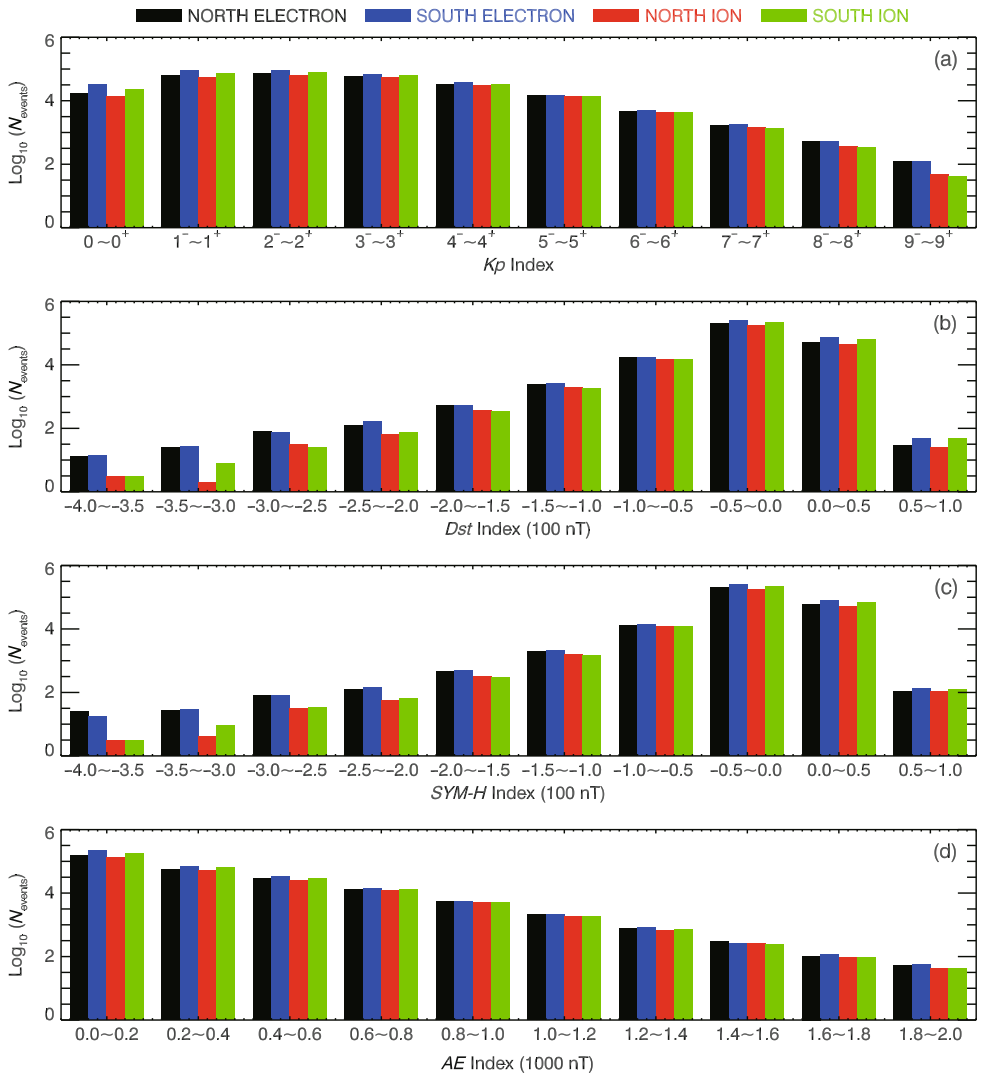

Figure 3 Histograms of the number of the events of B1E (black/blue) and B1I (red/green) in NH/SH hemisphere versus. (a) *Kp* (binned in 1 level intervals); (b) *Dst* (binned in 50 nT intervals); (c) *SYM-H* (binned in 50 nT intervals); (d) *AE* (binned in 200 nT intervals). To better display the events for disturbed periods, the vertical axes are all log-scaled since most of the events happen during quiet periods. The colors representing different boundaries are shown at top.

3 MLT and geomagnetic activity dependences

The MLT and geomagnetic activity dependences of the MLAT of B1E and B1I in both hemispheres are shown in Figure 4. According to the MLT coverage of the database in Figure 2(b), all the samples between 18:00–06:00 MLT are displayed, although the statistics in 00:00–04:00 MLT sector are disperse due to the low sampling by DMSP satellites compared with other sectors. Figure 4 shows that, as the enhancement of geomagnetic activity, both B1E and B1I in both hemispheres moves to low latitudes, from ~70° to ~55°; as the increase of MLT, both B1E and B1I in both hemispheres shift to low latitudes with the differences between B1E and B1I decreasing and B1I becomes poleward of B1E around 00:00 MLT, especially during high geomagnetic activities; and there are also some differences in conjugated hemispheres especially in the pre-midnight regions. There is a latitudinal increase around 21:00 MLT in NH for both B1E and B1I for all geomagnetic activities, while the decrease of MLAT in SH is somewhat monotonic.

4 Fitting to geomagnetic indices

Having known the basic information of the database and the dependences of MLAT on MLT and geomagnetic activity, we will fit the MLAT of B1E and B1I to *Kp*, *Dst*, *AE*, and *SYM-H* in this section to find the characteristics of variations.

The bin-averaged MLAT of B1E and B1I and their fittings to geomagnetic activities are shown in Figure 5. In Figure 5(a) the MLAT is linearly fitted to *Kp* in the form of MLAT = $A + B \times Kp$, and in Figure 5(b) and (d) the MLATs

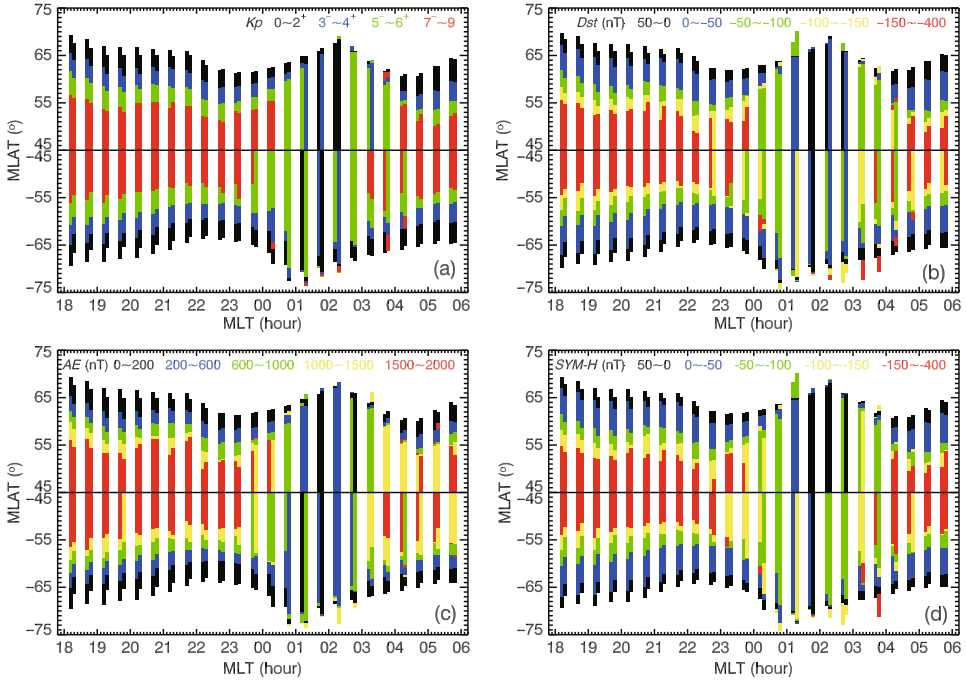

Figure 4 MLT and geomagnetic activity dependences of the MLAT of B1E and B1I in both hemispheres on *Kp* (a), *Dst* (b), *AE* (c), and *SYM-H* (d). The MLT is divided to 0.5 h bins with left for B1E and right for B1I in each bin. The colors representing the levels of geomagnetic activity are show at the bottom of each panel.

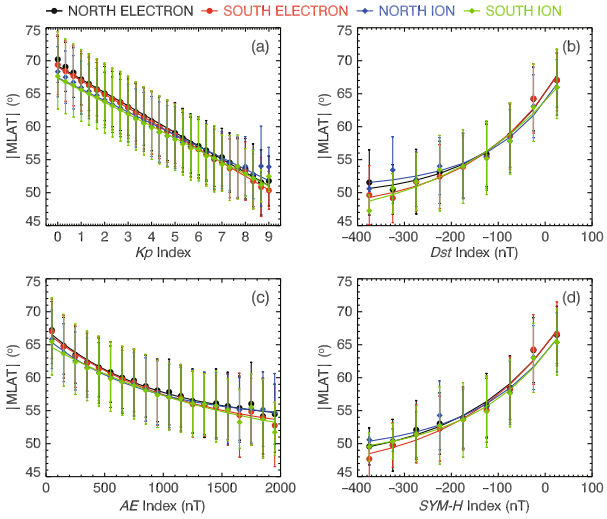

Figure 5 Average MLAT (symbols) of B1E and B1I and their fittings (solid curves) to geomagnetic indices *Kp* (a), *Dst* (b), *AE* (c), and *SYM-H* (d) in both hemispheres. The symbols represent the binned averages on *Kp* (binned in 0.33 intervals), *Dst* (binned in 50 nT intervals), *AE* (binned in 100 nT intervals), and *SYM-H* (binned in 50 nT intervals) with the error bars shown by the vertical lines. The colors and symbols representing different boundaries are shown at top.

are exponentially fitted to *Dst*, *AE*, and *SYM-H*, in the form of MLAT = $A_1 \times \exp(A_2 \times x) + A_3$, where x= *Dst*, *AE*, and *SYM-H,* respectively. The fitted parameters in above equations and the coefficients of determination (R^2, short for "*R*") are listed in Table 1. It is obviously shown in Figure 5 and Table 1 that as the increase of geomagnetic activity, both B1E and B1I move to low latitudes, in consistent with the latitudinal expansion of auroral oval during high geomagnetic activity (Feldstein et al., 1967; Newell et al., 1991). The MLAT of B1E is generally 2° larger than that of B1I, both of which move to 50° during high geomagnetic activity. In order to further understand the variation property in different MLT sectors, we have linearly fitted the MLAT to *Kp* in different MLT sectors.

The linear fittings of MLAT to *Kp* in MLT sectors of 1 h intervals are shown in Figure 6, the intercept A_0 and the slope K of the linear function MLAT=A_0+K×*Kp* and the corresponding coefficients of determination R are listed Table 2. We have also listed the results of Gussenhoven et al. (1987) in Table 3 for convenience of comparison. Since the data in 00:00–04:00 MLT sector are disperse according to Figure 4, fittings are not done in this sector.

Table 1 Fitting Parameters of MLAT to geomagnetic indices[a)]

	Kp			*Dst*				*SYM-H*				*AE*			
	A	*B*	*R*	A_1	A_2	A_3	*R*	A_1	A_2	A_3	*R*	A_1	A_2	A_3	*R*
NH B1E	69.21	–2.02	0.996	15.76	0.0065	49.26	0.973	17.91	0.0050	46.79	0.974	14.22	–0.0011	53.07	0.987
SH B1E	–69.04	2.07	0.979	–18.20	0.0054	–46.85	0.948	–19.79	0.0046	–44.96	0.960	–15.97	–0.0009	–50.93	0.995
NH B1I	67.42	–1.73	0.998	13.25	0.0071	50.63	0.976	15.11	0.0056	48.49	0.969	12.47	–0.0012	53.61	0.989
SH B1I	–67.33	1.81	0.994	–19.70	0.0039	–44.17	0.977	–15.81	0.0056	–47.77	0.976	–16.83	–0.0006	-48.29	0.962

a) *R* represents the linear correlation coefficients. The same below.

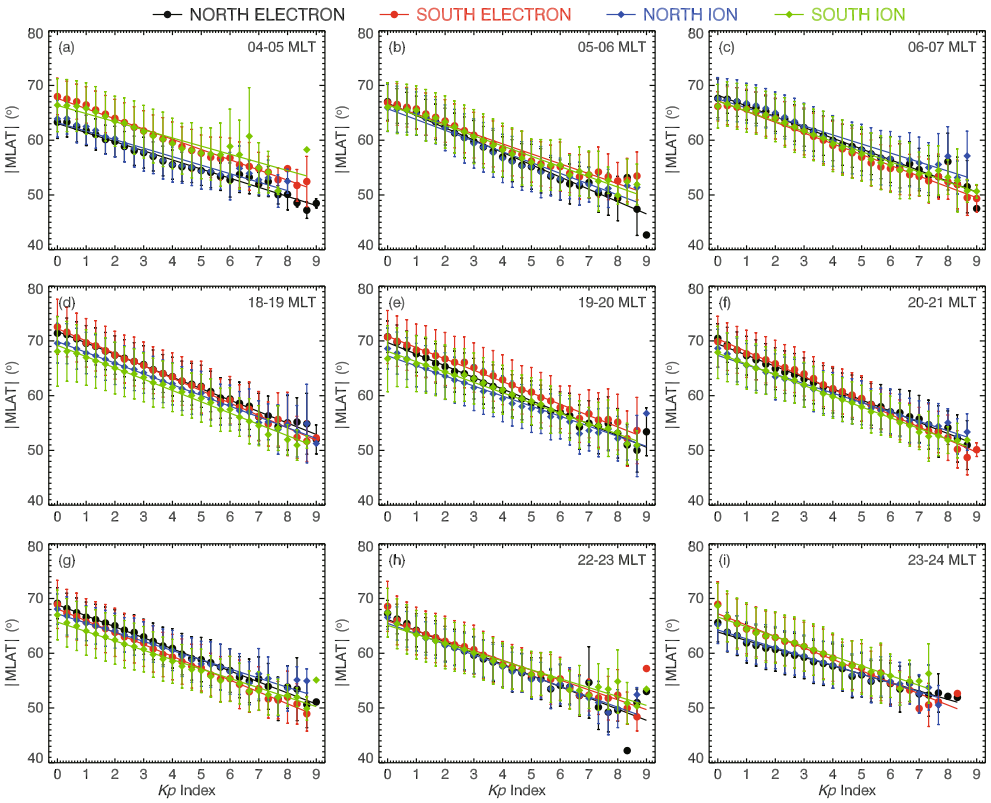

Figure 6 Linear fitting of MLAT to *Kp* at different MLT in both hemispheres. (a) 04:00–05:00 MLT, (b) 05:00–06:00 MLT, (c) 06:00–07:00 MLT, (d) 18:00–19:00 MLT, (e) 19:00–20:00 MLT, (f) 20:00–21:00 MLT, (g) 21:00–22:00 MLT, (h) 22:00–23:00 MLT, (i) 23:00–24:00 MLT. The symbols represent the binned averages on *Kp* (binned in 0.33 intervals) with the error bars shown by the vertical lines. The colors and symbols representing different boundaries are shown at top.

Table 2 *Kp* fitting in different MLT sectors

MLT sector	NH B1E			SH B1E			NH B1I			SH B1I		
	A_0	K	R	A_0	K	R	A_0	K	R	A_0	K	R
04:00–05:00	63.06	–1.67	0.988	–67.64	1.87	0.992	63.20	–1.55	0.970	–66.36	1.49	0.951
05:00–06:00	66.75	–2.25	0.978	–66.59	1.82	0.981	65.75	–1.97	0.980	–66.45	1.88	0.988
06:00–07:00	68.23	–1.97	0.990	–67.22	1.97	0.993	67.55	–1.65	0.982	–67.16	1.85	0.992
18:00–19:00	71.73	–2.09	0.997	–72.25	2.27	0.998	69.87	–1.97	0.996	–69.20	2.06	0.998
19:00–20:00	69.70	–2.12	0.991	–70.85	2.07	0.996	67.28	–1.84	0.986	–68.09	1.89	0.995
20:00–21:00	69.45	–2.05	0.996	–70.36	2.30	0.998	67.35	–1.72	0.992	–67.75	1.96	0.997
21:00–22:00	68.87	–2.01	0.989	–68.11	2.17	0.997	67.21	–1.68	0.961	–65.69	1.71	0.974
22:00–23:00	66.19	–2.05	0.947	–65.93	1.80	0.967	65.46	–1.92	0.984	–65.09	1.62	0.971
23:00–24:00	63.88	–1.54	0.991	–67.22	2.08	0.984	64.25	–1.61	0.989	–66.62	1.78	0.978

Table 3 Fitting results of Gussenhoven et al. (1987)

MLT sector	ELECTRON			ION		
	A_0	K	R	A_0	K	R
04:00–05:00	65.9	–1.68	–0.60	69.1	–1.96	–0.65
05:00–06:00	66.7	–1.62	–0.61	69.7	–1.59	–0.62
06:00–07:00	67.5	–1.57	–0.53	70.0	–1.30	–0.54
17:00–18:00	72.5	–1.45	–0.64	70.7	–1.40	–0.64
18:00–19:00	70.6	–1.16	–0.55	69.1	–1.20	–0.59
19:00–20:00	71.4	–2.01	–0.72	69.5	–1.75	–0.71
21:00–22:00	68.8	–1.17	–0.55	67.9	–1.10	0.55

Figure 6 and Table 2 show that: (1) in all MLT sectors, both B1E and B1I expand to low latitudes as *Kp* increases; (2) the MLAT differences between B1E and B1I change with MLT, B1E is poleward of B1I in both hemispheres in 05:00–07:00 MLT sector, B1E is slightly equatorward of B1I in 04:00–05:00 MLT sector in NH, B1E is ~2° poleward of B1I in both hemispheres in 18:00–23:00 MLT sector, and B1E is slightly equatorward of B1I in 23:00–24:00 MLT sector in NH; (3) the intercept decreases from 04:00 MLT to 07:00 MLT and from 18:00 MLT to 24:00 MLT, in consistent with the results in Table 3; (4) the slope is different in each MLT sector indicating that the variations of particle precipitation have clear MLT asymmetry. It is noted that the intercept in Table 2 is ~2° less than that in Table 3 for B1E and ~5° for B1I and the slopes in Table 2 are generally larger. The possible reasons are that the boundary of auroral precipitation is negatively correlated to solar activity (Hardy et al., 1987; He et al., 2014), and the data used by Gussenhoven et al. (1987) are just in January 1983 when the solar activity is low. In low solar activity, the MLAT of both B1E and B1I are larger and the slope is smaller.

5 Conclusions

Based on the auroral electron/ion precipitation boundary database observed by the DMSP satellites during 1984 and 2009, the latitudinal characteristics and geomagnetic activity (*Kp*, *Dst*, *AE*, and *SYM-H*) variations of B1E and B1I in both hemispheres are statistically investigated. The main results are as following.

The MALT of both B1E and B1I are located between 60°~70° in both hemisphere with the mean MLAT for B1E/B1I to be 64.30°N/63.22°N and 64.48°S/63.26°S in the NH and SH, respectively, indicating that B1E and B1I in both hemispheres are located in conjugated magnetic field lines with B1E ~1.2° poleward of B1I, in consistent with the value of 1.4° given by Gussenhoven et al. (1987).

As the geomagnetic activity enhances, B1E and B1I in both hemispheres shift to lower MLAT (from ~70° to ~55°). During different levels of geomagnetic activities, MLATs of both B1E and B1I and their differences slowly decrease from dusk to midnight with some difference in both hemispheres.

The MALTs of B1E and B1I in both hemispheres decrease linearly with *Kp* and exponentially with *Dst*, *AE*, and *SYM-H*, respectively, indicating that auroral particle precipitation is closely related with geomagnetic activity.

In different magnetic local time (MLT) sectors, the changing rates of the boundaries with *Kp* are different, and the rates of B1E are generally larger than that of B1I, indicating that the difference between B1E and B1I reduce with increasing geomagnetic activity.

This preliminary work provides us with a clear systematic understanding of the characteristics and geomagnetic activity variations of the auroral particle precipitations. The characteristics found in this paper are helpful to future modeling of the auroral precipitations. In future work, we will investigate the solar cycle, seasonal, diurnal variations of B1E and B1I and the relationship between auroral precipitation and plasmaspheric boundary by projection of B1E and B1I onto equatorial plane.

We sincerely thanks the help of National Satellite Meteorological Center China Meteorological Administration for data survey. The precipitation boundary database is provided by The Johns Hopkins University Applied Physics Laboratory (http://sd-www.jhuapl.edu/Aurora/dataset_list.html), and the geomagnetic indices (Kp, Dst, AE, and SYM-H) are provided by the Kyoto World Data Center (http://swdcwww.kugi.kyoto-u.ac.jp/index.html). This work was supported by the National Basic Research Program of China (Grant Nos. 2012CB957800, 2011CB811400), the National Hi-Tech Research and Development Program of China (Grant No. 2010AA121000), and the National Natural Science Foundation of China (Grant Nos. 41274147, 41204102).

Anderson P C, Johnston W R, Goldstein J. 2008. Observations of the ionospheric projection of the plasmapause. Geophys Res Lett, 35: L15110, doi: 10.1029/2008GL033978

Feldstein Y I, Starkov G V. 1967. Dynamics of auroral belt and polar geomagnetic disturbances. Planet Space Sci, 15: 209–229

Feldstein Y I, Galperin Y I. 1985. The auroral luminosity structure in the high-latitude upper atmosphere: Its dynamics and relationship to the large-scale structure of the earth's magnetosphere. Rev Geophys, 23: 217–275

Feldstein Y I, Galperin Yu I. 1996. The auroral precipitation structure in the nighttime magnetosphere. Cosmic Res, 34: 227–247

Gussenhoven M S, Hardy D A, Burke W J. 1981. DMSP/F2 electron observations of equatorward auroral boundaries and their relationship to magnetospheric electric fields. J Geophys Res-Space Phys, 86: 768–778

Gussenhoven M S, Hardy D A, Heinemann N. 1983. Systematics of the equatorward diffuse auroral boundary. J Geophys Res-Space Phys, 88: 5692–5708

Gussenhoven M S, Hardy D A. 1987. The equatorward boundary of auroral ion precipitation. J Geophys Res-Space Phys, 92: 3273–3283

Hardy D A, Yeh H C, Schmitt L K, et al. 1984. Precipitating electron and ion detectors (SSJ/4) on the block 5D/Flights 6-10 DMSP satellites: Calibration and data presentation. Air Force Geophys Lab Tech Rep, AFGL-TR-84-0317

Hardy D A, Gussenhoven M S, Raistrick R, et al. 1987. Statistical and functional representations of the pattern of auroral energy flux, number flux, and conductivity. J Geophys Res-Atmos, 92: 12275–12294

He F, Zhang X X, Chen B. 2014. Solar cycle, seasonal, and diurnal variations of subauroral ion drifts: Statistical results. J Geophys Res-Space Phys, 119, doi: 10.1002/2014JA019807

Horwitz J L, Menteer S, Turnley J, et al. 1986. Plasma boundaries in the inner magnetosphere. J Geophys Res-Space Phys, 91: 8861–8862

Nakai H, Kamide Y, Hardy D A, et al. 1986. Time scales of expansion and contraction of the auroral oval. J Geophys Res-Space Phys, 91: 4437–4450

Newell P T, Wing S, Meng C I, Sigillito V. 1991. The auroral position, structure, and intensity of precipitation from 1984 onwards: An automated online data base. J Geophys Res-Space Phys, 96: 5877–5882

Newell P T, Feldstein Y I, Galperin Y I, et al. 1996. The morphology of nightside precipitation. J Geophys Res-Space Phys, 101: 10737–10748

Newell P T, Ruohoniemi J M, Meng C I. 2004. Maps of precipitation by source region, binned by IMF, with inertial convection streamlines. J Geophys Res-Atmos, 109, doi: 10.1029/2004JA010499

Xu W Y. 2009. Physics of Electromagnetic Phenomena of the Earth. Hefei: University of Science and Technology of China Press. 45